Theoretical study of the ionization of liquid water from its several initial orbitals by fast electron impact

2015 J. Phys. B: At. Mol. Opt. Phys. 48 155201

(http://iopscience.iop.org/0953-4075/48/15/155201)

IOP Publishing Journal of Physics B: Atomic, Molecular and Optical Physics

J. Phys. B: At. Mol. Opt. Phys. **48** (2015) 155201 (10pp) doi:10.1088/0953-4075/48/15/155201

Theoretical study of the ionization of liquid water from its several initial orbitals by fast electron impact

M L de Sanctis[1], M-F Politis[2], R Vuilleumier[3], C R Stia[1] and O A Fojón[1]

[1] Instituto de Física Rosario, CONICET-Universidad Nacional de Rosario, Bvd. 27 de Febrero 210 bis, 2000 Rosario, Argentina
[2] Laboratoire Analyse et Modélisation pour la Biologie et l'Environnement, CNRS UMR 8587, Université d'Evry Val d'Essone, Boulevard François Mitterrand, F-91025 Evry, France
[3] École Normale Supérieure, Département de Chimie, UMR 8640 CNRS-ENS-UPMC, 24, rue Lhomond, F-75005 Paris, France

E-mail: fojon@ifir-conicet.gov.ar

Received 26 February 2015, revised 7 April 2015
Accepted for publication 28 April 2015
Published 26 June 2015

Abstract

We theoretically study the single ionization of liquid water by energetic electrons through one active-electron first-order model. We analyze the angular ejected electron spectra corresponding to the most external orbitals $1B_1$, $2A_1$, $1B_2$ and $1A_1$ of a single water molecule. We work to create a realistic description of those orbitals corresponding to single molecules in the liquid phase. This goal is achieved by means of a Wannier orbital formalism. Multiple differential cross sections are computed and compared with previous calculations for both liquid and gas phases. In addition, our present results are integrated over all orientations and compared with experimental ones for randomly oriented vapour water molecules, as no experiments currently exist for the liquid phase. Moreover, we estimate the influence of the passive electrons on the reaction by means of a model potential.

Keywords: ionization, liquid water, electron impact

(Some figures may appear in colour only in the online journal)

1. Introduction

The ionization of water molecules is an important process in several areas such as nuclear reactors, plasma physics, astrophysics, medical physics and radiobiology. In the latter, water plays a determinant role because the biological tissue is largely composed of water in the condensed phase. The irradiation of liquid water molecules may lead to the production of radicals and/or ionic species that could react with the solvated molecules of the medium. This in turn may bring about a wide spectrum of damages in the macromolecules such as the DNA or RNA leading to cell death, cell transformation and gene mutation.

In studying charge transfer reactions at the basic level, the multiple differential cross sections (MDCS) bring the most detailed information on the mechanisms involved. Particularly, angular distributions of secondary electrons allow the determination of the preferential directions or energies at which electrons are ejected as a result of ionization of the target. So, reliable cross sections for the interactions between electrons (as well as other charged particles) and water reveal a useful tool to unravel the energy deposition in matter. However, due to the experimental difficulties in dealing with liquid water there is a lack of experimental results for this target. The main reason for this paucity of aqueous data in collision reactions is due to the high vapour pressure preventing from reaching a good vacuum condition necessary to conduct other way standard experiments. Nevertheless, in recent years a new experimental technique was implemented to measure secondary ion emission by light heavy ion impact from various liquid targets such as water and ethanol [1–5]. In such liquid-in-vacuum experiments

analogous to the well established ones coming from the laser domain [6, 7], heavy projectiles are passsed through a molecular liquid target microjet prepared in vacuum. In this way, the first results for ion-fragment yields by impact of massive projectiles were obtained [1–5]. Besides, due to the complexities in theoretically describing the aqueous phase, most of the track structure studies used vapour water to model the biological environment. In this context, a realistic description of the water molecules in the liquid phase is desirable.

Here, we study the single ionization of liquid water molecules by the impact of fast electrons properly describing the initial condensed phase. An isolated water molecule is considered as the target in most of the previous studies with electrons or heavy projectiles [8–29]. Only a few ones addressed the study of liquid water [19, 30–39]. In our recent work [38] (hereafter referred to as I), MDCS for the most external $1B_1$ liquid water orbital were obtained by using the first Born approximation. Within the framework of an independent electron approximation, it was assumed that one of the target electrons (the *active* one) is ejected in the final channel of the reaction, whereas the other ones (the passive electrons) remain as frozen in their initial states. This approximation is supported by the fact that at high enough incidence energies it can be supposed that there is no appreciable relaxation of the target during the effective collision time. The model reduces then the many-electron problem to an independent-single electron one.

A key ingredient of the model presented in I is that the $1B_1$ wavefunction of a single water molecule in the liquid phase is represented in a realistic way through the use of a Wannier orbitals formalism (see I and references quoted therein). The model was used with success to describe the main physical features observed in measured MDCS for randomly oriented vapour water molecules [14, 18], showing also a reasonable good agreement with previous theoretical MDCS for both liquid [19] and gas phases [17, 19]. However, this good accord may not be enough to conclude that the basic hypothesis of our model is suitable to describe the reaction of interest. Therefore, additional theoretical work is needed in order to obtain more conclusive evidence. In this way, we contrast our predictions in different situations considering other orbitals and estimate to what extent the effect of the passive electrons on the reaction is relevant. Here, we report new single ionization results for the $2A_1$, $1B_2$ and $1A_1$ orbitals. Computations of MDCS are performed for fixed-in-space as well as randomly oriented water molecules both in the liquid phase. In addition, the influence of the *passive* electrons is estimated by including a simple effective potential in the perturbation in the entrance channel of the reaction.

The paper is organized as follows: the theoretical method is described shortly in section 2. The results are presented and discussed in section 3 and the conclusions are given in section 4. Atomic units are used if not otherwise explicitly stated.

2. Theory

We outline here the main points of the theoretical procedure, giving also a description of the bound states of the liquid water as it will be useful in the results section.

To represent the reaction of interest, we employ the prior version of the transition matrix element

$$t_{fi}^{e} = \left\langle \Psi_f^- \,\middle|\, V_i \,\middle|\, \psi_i \right\rangle, \tag{1}$$

where ψ_i is the electronic wavefunction in the initial channel and Ψ_f^- is the final electronic wavefunction with correct asymptotic conditions. V_i is the perturbation in the entrance channel.

2.1. Initial state

The initial wavefunction is chosen as a product of a plane wave for the incident electron and a bound molecular wavefunction,

$$\psi_i = \frac{e^{i\mathbf{k}_i.\mathbf{R}}}{(2\pi)^{3/2}} \Phi_i(\mathbf{r};\, \alpha,\, \beta,\, \gamma), \tag{2}$$

where $\mathbf{R}$ and $\mathbf{r}$ are the position vectors of the incident electron and the active electron, respectively, with respect to the center of mass of the molecule. Moreover, $\mathbf{k}_i$ denotes the incident electron momentum whereas α, β and γ are the Euler angles defining the orientation of the molecule.

The molecular orbital Φ_i corresponding to a single water molecule in the liquid phase is obtained through the scheme introduced by Vuilleumier and co-workers [40, 41]. The liquid phase is simulated by a periodically repeated cubic cell of dimension 30 au containing 128 water molecules, which reproduce the experimental density under ambient conditions. The choice of such relatively big simulation box allows us to obtain proper wavefunctions that almost vanishes at and beyond the box walls (see I and references therein), that is essential to perform realistic cross sections calculations.

The electronic state of the whole sample is described in the framework of the Kohn–Sham density functional theory. From the occupied, extended, Kohn–Sham orbitals for a pure liquid water, the molecular wavefunctions Φ_i used in this work are constructed as follows (see [40, 41] for details). First, maximally localized Wannier functions w_n are attributed to molecules through a unitary transformation $\mathbf{U}$ of the occupied Kohn–Sham orbitals ψ_k,

$$w_n = \sum_k U_{nk} \psi_k \tag{3}$$

in such a way that the spatial spread of the resulting orbitals is minimized [42]. Thus, four doubly occupied Wannier orbitals can be assigned to each water molecule of the liquid: two of them representing OH bonds and the other two ones describing lone pairs [43]. Second, these Wannier functions associated to a molecule are used as a basis for effective molecular orbitals for this molecule. It is achieved by grouping the Wannier orbitals of a specific molecule and then rediagonalizing by molecular blocks the Wannier Hamiltonian [40, 41]. The resulting orbitals Φ_i can be thus

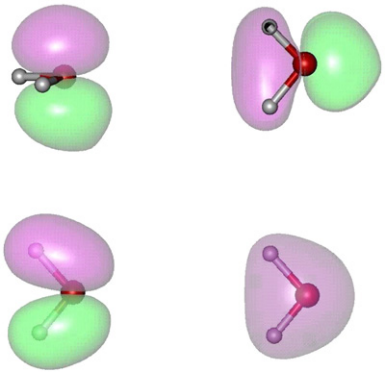

Figure 1. Effective molecular orbitals of a single water molecule of the liquid. Top left panel $1B_1$, top right panel $2A_1$, bottom left panel $1B_2$ and bottom right panel $1A_1$.

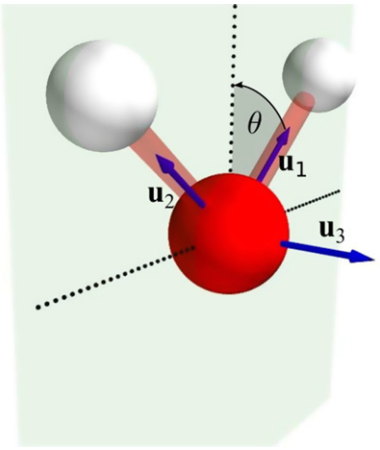

Figure 2. Unit vectors for a single water molecule used in the text.

expressed as

$$\Phi_i = \sum_n T_{in}\ w_n, \tag{4}$$

where the summation is restricted to the valence orbitals of a single probe molecule. Here, $\mathbf{T}$ represents the corresponding unitary transformation. As a consequence, four effective doubly occupied molecular orbitals Φ_i per water molecule are obtained which can be unambiguously labeled $1A_1$, $1B_2$, $2A_1$ and $1B_1$ by similarity with the standard orbitals for isolated water molecules. The average ionization energies given by this procedure are equal to 25.66, 13.15, 10.24 and 8.2 eV, respectively.

Calculated effective molecular orbitals for the selected water molecule in the liquid phase are drawn in figure 1. The molecular plane contains the unit vectors $\mathbf{u}_1$ and $\mathbf{u}_2$ pointing along the O–H bonds directions, the unit vector $\mathbf{u}_3$ is normal to this plane, and θ is the half angle between $\mathbf{u}_1$ and $\mathbf{u}_2$ (see figure 2). The liquid phase orbitals are similar to the ones of the gas phase although the C_{2v} symmetry is broken. For instance, the $1B_1$ orbital presents a high directional p-like character, possessing a nodal plane in the molecular plane. The $1B_2$ orbital presents also a high p character with a nodal plane perpendicular to the molecular plane passing by the oxygen atom. The $2A_1$ orbital exhibits also a p-like behaviour and its charge density is concentrated at both sides of the oxygen atom, showing a lobe which surrounds the H atoms and other one in the opposite direction. In contrast, the $1A_1$ orbital has mainly an atomic s-like character with some degree of asymmetry. The charge distribution of this orbital is accumulated in the region around and between the three nuclei reaching its greater values near the molecular plane and around the H atoms.

2.2. Final state

The final-state wavefunction is chosen as

$$\Psi_f^- \cong \frac{\mathrm{e}^{\mathrm{i}\mathbf{k}_s.\mathbf{R}}}{(2\pi)^{3/2}} C\left(\mathbf{k}_e, \mathbf{r}, \nu\right), \tag{5}$$

where $\mathbf{k}_s$ and $\mathbf{k}_e$ are the momenta of the scattered electron and the active ejected one, respectively. In addition, the continuum Coulomb wavefunction given by

$$C(\mathbf{k}, \mathbf{r}, \nu) = \Gamma(1 - \mathrm{i}\nu)\ \frac{\mathrm{e}^{\mathrm{i}\mathbf{k}_e.\mathbf{r}}}{(2\pi)^{3/2}} \times \mathrm{e}^{-\pi\nu/2}\ {}_1F_1[\mathrm{i}\nu;\ 1;\ -\mathrm{i}(kr + \mathbf{k}.\ \mathbf{r})] \tag{6}$$

describes the ionized electron in the final channel in the field of the residual target at asymptotically large distances. ${}_1F_1$ is the confluent hypergeometric function and $\nu = -Z^*/k$ is the corresponding Sommerfeld parameter. Here, Z^* is the effective charge corresponding to the residual target seen by the active electron. At asymptotic large distances, the charge $Z^* = 1$ corresponds to a total screening of the charge of the nuclei of the molecule by the passive electrons, giving as a result of a residual target with a net charge equal to unity.

2.3. Perturbation potential

According to the choice of the initial state, the perturbation V_i in the initial channel is taken as

$$V_i = \frac{1}{r_p} - \frac{1}{R}, \tag{7}$$

where $\mathbf{r}_p = \mathbf{r} - \mathbf{R}$ is the position vector of the active electron with respect to the projectile. The perturbation V_i corresponds to the interaction of the projectile with the *active* electron ($1/r_p$) and with a net charge equal to unity concentrated in the mass-center of the molecule ($-1/R$). This is compatible with the complete screened charge of the nuclei by the passive electrons. Furthermore, the spatial distribution of the nuclei and passive electrons in the water molecule is neglected in the last expression and replaced by an average of the interaction of the projectile with these particles. This approximation was employed in I for the case of the ionization from the most external $1B_1$ orbital as well as in previous studies for the ionization of multielectronic targets ([44], see also [45] for a review) and even for liquid water [19].

2.4. Cross sections

The eight-fold differential cross sections (8DCS) for the single ionization of a fixed-in-space water molecule in the liquid phase may be obtained as

$$\sigma^{(8)}(\alpha, \beta, \gamma) = \frac{\mathrm{d}\sigma}{\mathrm{d}\Omega_{\mathrm{mol}}\mathrm{d}\Omega_e\mathrm{d}\Omega_s\mathrm{d}E_e} = N(2\pi)^4\frac{k_e k_s}{k_i}\left|t_{fi}^{e}\right|^2, \quad (8)$$

where the *active* electron is ejected with momentum k_e (and energy E_e) into the differential solid angle Ω_e with respect to the incidence direction (defined by $\mathbf{k}_i$), and the projectile is scattered with momentum $\mathbf{k}_s$ into the solid angle Ω_s. In equation (8), $\mathrm{d}\Omega_{\mathrm{mol}} = \sin\beta\ \mathrm{d}\alpha\ \mathrm{d}\beta\ \mathrm{d}\gamma$, being α, β, γ the Euler angles of the water molecule. Moreover, as exchange effects are not taken into account, $N = 2$ gives the number of electrons in the initial molecular orbital.

Finally, integrating the 8DCS given by the equation (8) over the Euler angles, we obtain five-fold differential cross sections (5DCS) averaged over all possible molecular orientations

$$\sigma^{(5)} = \frac{\mathrm{d}\sigma}{\mathrm{d}\Omega_e\mathrm{d}\Omega_s\mathrm{d}E_e} = \frac{1}{8\pi^2}\int\sigma^{(8)}(\alpha, \beta, \gamma)\sin\beta\ \mathrm{d}\alpha\ \mathrm{d}\beta\ \mathrm{d}\gamma. \quad (9)$$

To compute the 8DCS and 5DCS, numerical quadratures are performed within the simulation box.

3. Results

We calculate MDCS for single ionization of liquid water molecules from their four external orbitals. Asymmetric kinematic conditions for scattered and ejected electrons (ejection energies of some eV) are considered. The collision takes place in a coplanar geometry in which incident, scattered and ejected electron momenta lie all in the same plane. Firstly, differential cross sections for fixed molecular orientations are presented. Secondly, 5DCS for averaged oriented water molecules are presented and compared with measurements for the gas phase [14], as no experimental results exist for the liquid water molecule yet. Results are compared also with previous calculations for both liquid [19] and gas phases [17, 19].

3.1. MDCS for fixed molecular orientation: 8DCS

In this section, 8DCS for oriented water molecules in liquid phase are presented as a function of the ejection angle θ_e. The incident and ejection energies are $E_i = 250$ eV and $E_e = 5$ eV, respectively. We consider here three particular arrangements in which the molecule is oriented either perpendicularly or parallel to the collision plane defined by both the $\mathbf{k}_i$ and $\mathbf{k}_s$ momenta directions. These configurations are denoted as *normal I* , *normal II* and *coplanar*, and are illustrated in figures 3(a)–(c), respectively. Thus, for the *normal I* (*II*) orientation the molecular plane is contained in the *xy* (*yz*) plane whereas for the *coplanar* orientation the molecule lies in the collision plane (*xz* plane). These orientations correspond to the Euler rotations $R_0(\theta, 0°, 0°)$, $R_0(\theta, 90°, 180°)$ and $R_0(\theta - 90°, 90°, -90°)$, respectively. The rotation operator is defined as $R_0(\alpha, \beta, \gamma) = R_{z''}(\gamma)R_{y'}(\beta)R_z(\alpha)$ [46].

To the best of our knowledge no cross sections for oriented water molecules exist neither experimentally nor theoretically, except for the calculations presented in [13] for the gas phase. Unfortunately, those predictions were performed by including only the $1/r_p$ term instead of the full perturbation given by equation (7). In I, liquid 8DCS obtained with the single $1/r_p$ contribution are tested with the ones for the gas [13] for ionization from the $1B_1$ orbital. A rather good agreement is found between both calculations [38]. Although not shown here, similar calculations for the ionization from several initial orbitals of oriented liquid water molecules have been performed, showing also a qualitative accord with those partial angular distributions reported for the gas phase. Nevertheless, the full perturbation given by equation (7) is required in order to obtain MDCS that represent in a proper way the physics involved in the reaction. Actually, even if the $1/r_p$ term is crucial to describe the classical mechanism that gives rise to the binary peak, the neglected $1/R$ term in [13], for instance, plays a major role in the description of the recoil peak. As we will show below, both binary and recoil peaks appear as clear fingerprints in randomly oriented MDCS at the kinematics of interest of this work.

Therefore, liquid phase 8DCS obtained with the full perturbation given by equation (7) are presented here for fixed scattering angles $\theta_s = 0°$ and $\theta_s = 15°$. At small scattering angles, the momentum transfer $\mathbf{q} = \mathbf{k}_i - \mathbf{k}_s$ is small ($q = 0.11$au for $\theta_s = 0°$) and the ionization process can be considered as mostly dipolar. In this case, the projectile electron is sensitive to the whole electronic distribution and, consequently, to the spatial orientation of the molecule. As pointed out in I for the *normal I* configuration, ionization from the $1B_1$ orbital is favoured along in its *p*-direction whereas the electron emission decreases in its nodal plane [38]. Analogous results are found here for the $1B_1$ and $2A_1$ orbitals in the *normal II* configuration, taking into account their directionality (figures 4(a) and (b)). The cross sections obtained with the full perturbation (full line) present additional structures due to the coherent sum of both the $1/r_p$ and $1/R$ contributions (respectively, dotted and dashed lines in figures 4(a)–(c)). However, it is worth mentioning that some of these structures might disappear if higher orders terms than the first one were considered in the calculation. We do not include results for the $1B_2$ orbital as they can be considered as negligible. This is due to the fact that the nodal plane of this orbital coincides with the collision plane when the molecule is in the normal orientations.

In the case of the *s*-like $1A_1$ orbital (figure 4(c)), the minima for both the $1/r_p$ and $1/R$ terms appear at different angular positions in contrast with the behaviour observed for the *p*-type orbitals.

To evaluate the effect of the molecular orientation, cross sections obtained with the full perturbation for the different

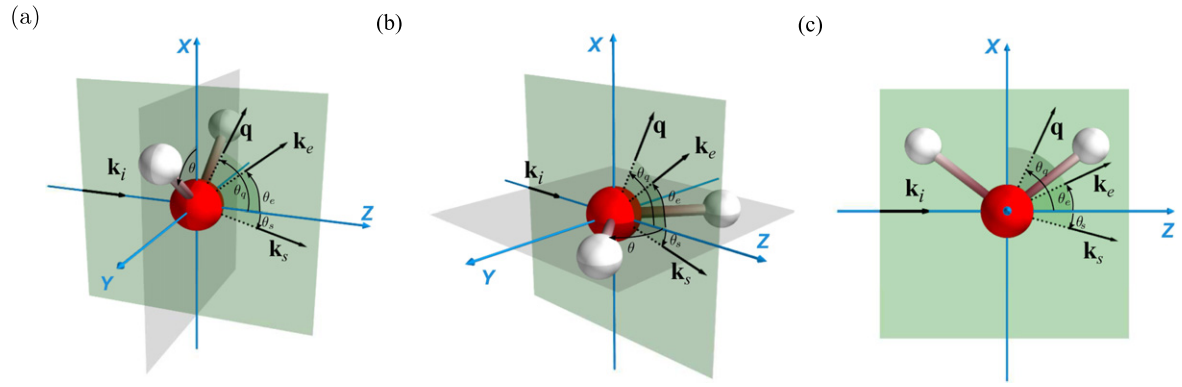

Figure 3. Fixed-in-space molecule orientations considered in this work. (a) *Normal I* . (b) *Normal II* . (c) *Coplanar*. The collision plane coincides with the *xz* plane.

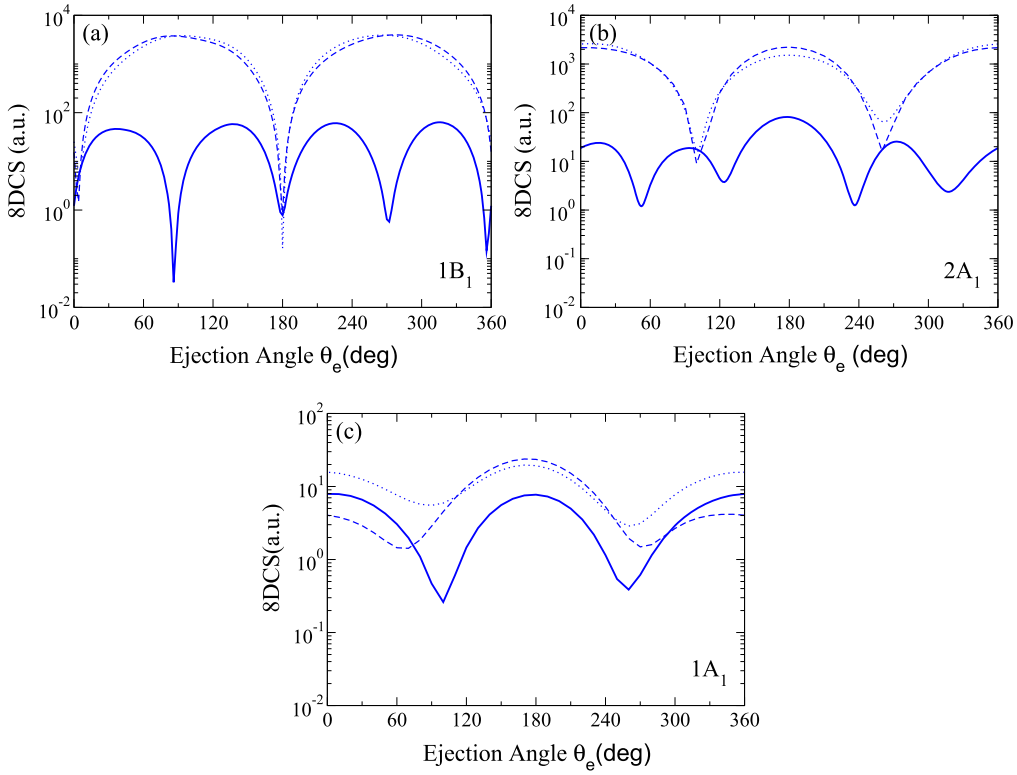

Figure 4. 8DCS per electron for different initial orbitals and the molecule oriented in the *normal II* configuration. The incidence and the ejection energies are $E_i = 250$ eV and $E_e = 5$ eV, respectively, and $\theta_s = 0°$. Full line: full perturbation. Dashed line: $1/R$ contribution. Dotted line: $1/r_p$ contribution.

orbitals are presented in figures 5(a)–(d) for the same configurations and kinematics considered above. The results for the *normal II* alignment shown in figure 4 are also included here for the sake of completeness. In the case of the $1B_1$ orbital and for the *normal I* orientation (figure 5(a), dashed line), relative maxima are observed at $\theta_e = 0°$ and 180° (in the directions of the orbital alignment) as well as other minor structures coming from the interplay of both terms of the perturbation. Indeed, it is found that the cross section profile is shifted approximately 90° respect to the one for the *normal II* configuration (figure 5(a), full line). For the *coplanar* arrangement (not shown here), calculations are almost two orders lower than the ones for the normal orientations considered before. Analogous considerations apply to the cases of the $2A_1$ and $1B_2$ orbitals. For instance, $2A_1$ cross sections for both *coplanar* and *normal I* arrangements (figure 5(b), dotted and dashed lines, respectively) present quite similar patterns due to the fact that the $2A_1$ orbital lies along the *x*-axis in both configurations. In figure 5(c), $1B_2$ results are shown only for the *coplanar* orientation since the contribution from the normal configurations are negligible. Concerning the $1A_1$ orbital (figure 5(d)), results exhibit essentially the same features observed in figure 4(c) for the *normal II* configuration, showing a no significant dependence on the molecular alignment. It is in agreement with the expected behaviour of a *s*-like atomic orbital (at $\theta_s = 0$)

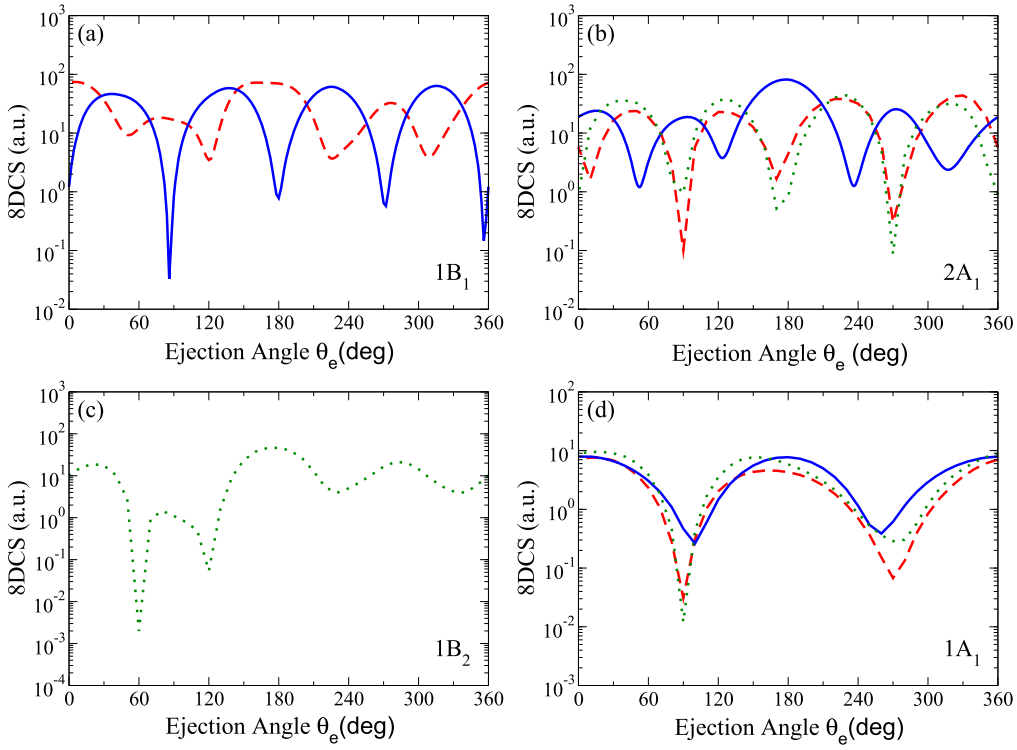

Figure 5. Full 8DCS per electron for the different orbitals at the definite orientations of the molecule given by figure 3. Same kinematic conditions as in figure 4. Dashed line: *normal I* orientation. Full line: *normal II* orientation. Dotted line: *coplanar* orientation.

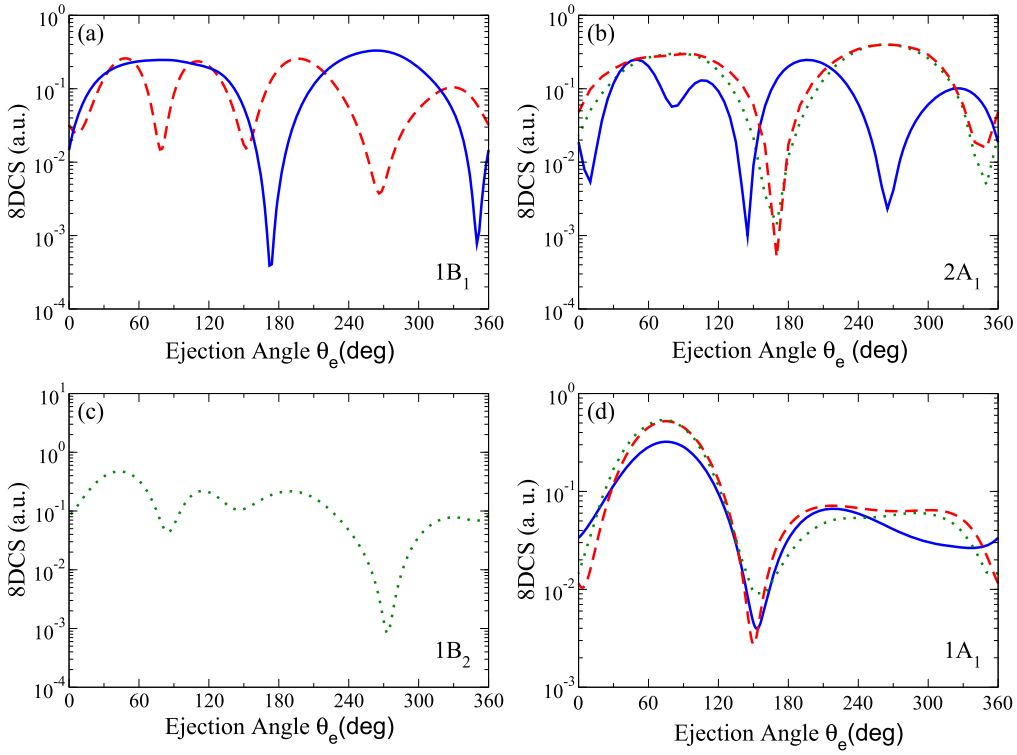

Figure 6. Same as figure 5 but $\theta_s = 15°$.

where the target electrons are ejected preferably at forward and backward directions.

In figures 6(a)–(d), we show 8DCS results for scattering angle $\theta_s = 15°$. Under such kinematic conditions, the momentum transfer is larger ($q = 1.1$ a.u.) than in the preceding case for $\theta_s = 0$, and the ionization process is expected to exhibit the typical features of a binary collision regime. In this context, electron ejection increases preferably at around

the classical directions given by the momentum transfer direction $\theta_e \approx 75°$ and approximately the opposite one, i.e., $\theta_e \approx 255°$. Cross sections as a function of the ejection angle are supposed to present mainly two peaks, the well-known binary and recoil peaks, at those positions. For the case of the $1B_1$, $2A_1$ and $1B_2$ orbitals (figures 6 (a)–(c), respectively), 8DCS profiles present features which correspond to *p*-like orbitals [47]. In particular, when one of these orbitals is directed along the incidence direction at the kinematic conditions considered, a two-lobe structure appears at around the binary peak region. For instance, for the case of the $1B_1$ orbital and for the *normal I* orientation (figure 6(a), dashed line), minima are observed at the binary peak position and at about the opposite direction. Similar behaviour is found for the $2A_1$ orbital when the molecule is oriented in the *normal II* configuration (figure 6(b), full line), and also for the $1B_2$ orbital lying along the collision plane (figure 6(c), dotted line). It can be shown that this behaviour comes from the $1/r_p$ term of the interaction which is essential in the description of the classical mechanism that gives place to the binary peak. However, as stated before, 8DCS distributions are determined by the contribution of both terms of the perturbation given by equation (7) as well as the marked directionality of the *p*-like orbitals. Finally, the $1A_1$ orbital present a binary peak characteristic of *s*-like orbitals located at about the momentum transfer direction ($\theta_e = 68°$). In this case, the cross sections show no major dependence on the molecule orientation.

3.2. MDCS averaged over all molecular orientations: comparison between liquid and gas results

In this section we present 5DCS corresponding to each molecular orbital of the liquid water as a function of the ejection angle θ_e. Calculations are carried out for incident and ejected electron energies of $E_i = 250$ and $E_e = 10$ eV (except for the $2A_1$ orbital for which the ejected electron energy is of 8 eV), respectively.

The kinematic regime is the same as the one for the experiments performed for randomly oriented water vapour molecules [14]. Previous theoretical results for both gas [17, 19] and liquid [19] phases are also considered to contrast with our findings when possible.

To gain further insight into the reactions, we take into account in a simple way the repulsion between the active electron and the passive ones in the initial channel of the reaction. Previously, we tested several model potentials for the case of ionization of the most external $1B_1$ orbital and we concluded that a simple model potential with screened charges following the Slater's rules seems to be the more judicious choice [48]. According to this, the short-range potential V_s given by,

$$V_s(R) = -\sum_j N_j \frac{1}{R} \exp\left(-2Z_j^{\text{eff}} R\right)\left(1 + Z_j^{\text{eff}} R\right) \qquad (10)$$

is added in the perturbation given by equation (7). Here, $Z_j^{\text{eff}} = Z - S_j$ is an effective atomic charge, being $Z = 10$ and S_j the screening constant based on Slater's rules [49]. In equation (10), the summation runs over the j different water orbitals where N_j is the corresponding occupation number. It is easy to verify that the potential given in equation (10) satisfies the expected asymptotic conditions.

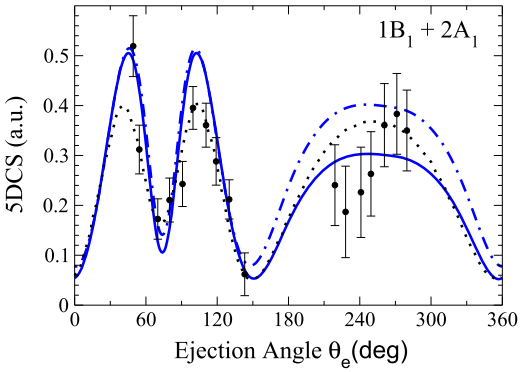

Figure 7. Summed 5DCS for the $1B_1$ and $2A_1$ orbitals for incident energy $E_i = 250$ eV, ejected electron energy $E_e = 10$ eV, and scattering angle $\theta_s = 15°$. Full line: present liquid phase results. Dashed–dotted line: present liquid calculations including the potential V_s (equation (10)) in the perturbation. Dots: normalized gas phase measurements for the summed $1b_1$ and $2a_1$ orbitals [14]. Dotted line: 1CW gas phase results [17].

In figure 7, we show our 5DCS corresponding to the summed contributions of both $1B_1$ and $2A_1$ orbitals (full line) as a function of the emitted electron angle θ_e. The angular distribution shows mainly the binary and recoil structures located at around the expected classical angles given by the directions of $\mathbf{q}$ and $-\mathbf{q}$. Indeed, the well known double-lobe structure appearing at forward emission angles (binary region) is consistent with the strong *p* character associated to both $1B_1$ and $2A_1$ outer orbitals. Although the inclusion of the static potential V_s does not affect the 5DCS profiles (dashed–dotted line) at the binary region, it is responsible of an appreciable enhancement (of about 30%) of the recoil peak. In figure 7, we include also experimental [14] and theoretical [17] results for the gas phase. As the measurements were obtained on a relative scale [14], we have normalized them conveniently to the gas calculations in the binary region to make a comparison. At variance with the binary region, the experiments are not able to resolve in energy the separate contribution from the $1b_1$ and $2a_1$ water vapour orbitals at the recoil region. Present results for the liquid show a qualitative good agreement with the experiments for the gas although some differences exist mainly at the binary region. More precisely, the liquid 5DCS profile presents an almost symmetric two-lobe structure in the binary region whereas a marked dissimmetry is observed in the measurements for the gas. A reasonable accord is found also between our results and the theoretical ones for the gas (dotted line) obtained in the framework of the 1CW model [17]. In this approximation, the initial state is represented by a product of a plane wave for the incident electron and the Moccia's molecular wavefunction [51] for the bound state of the target in the gas phase. In turn, the final state wavefunction is described as the product of a plane wave for the scattered electron and a Coulomb wavefunction with effective ionic charge $Z^* = 1$ for the ionized electron. There is a general similar behaviour between

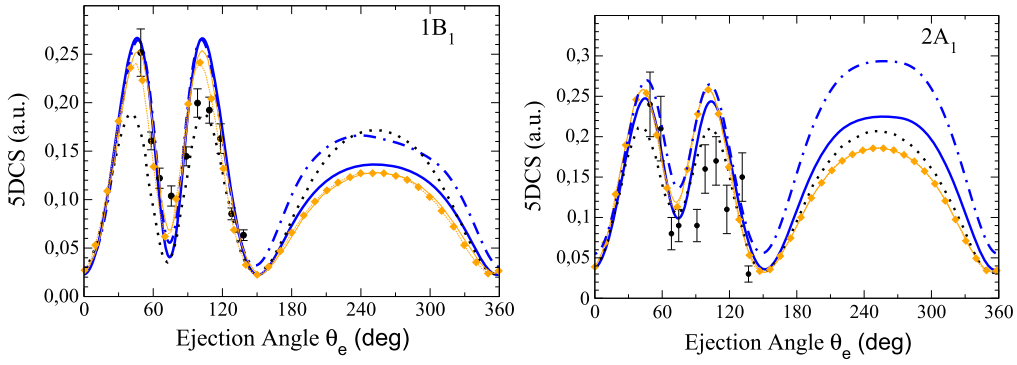

Figure 8. Same as figure 7 but for the ionization from the separate $1B_1$ and $2A_1$ orbitals. The ejection energies are $E_e = 10$ eV for the $1B_1$ orbital and $E_e = 8$ eV for the $2A_1$ one. Thin full-line: liquid FBA-CW results [19]. Full diamonds: gas FBA-CW results [19].

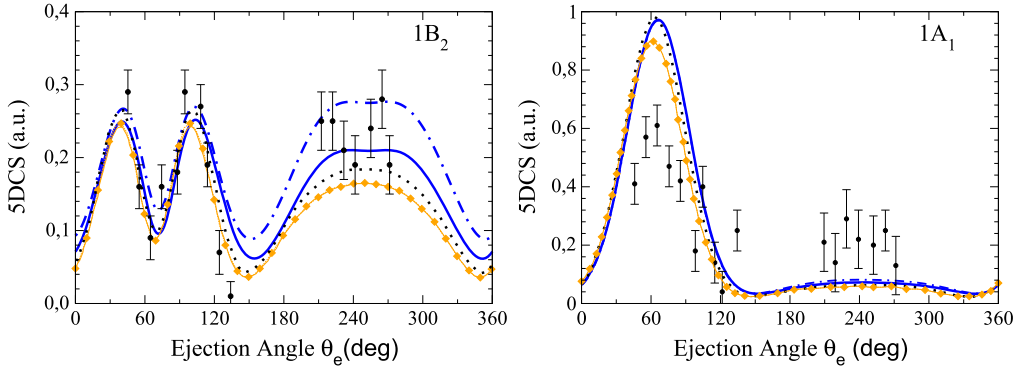

Figure 9. 5DCS for the $1B_2$ and $1A_1$ orbitals for incident energy $E_i = 250$ eV, ejected electron energy $E_e = 10$ eV, and scattering angle $\theta_s = 15°$. Full line: present liquid phase results. Dashed–dotted line: present liquid calculations including the potential V_s (equation (10)) in the perturbation. Dotted line: 1CW gas phase results [17]. Thin full-line: liquid FBA-CW results [19]. Full diamonds: gas FBA-CW results. Dots: normalized gas phase measurements [14].

our results and the 1CW ones for the vapour. However, we observe that the height of the two-lobe structure for the gas phase at the binary region is approximately 20% lower than the one predicted by our model for the liquid phase. In contrast, it is found that the gas 1CW results are greater than ours for the liquid without static potential in the recoil region. The inclusion of the static potential in our calculations gives a recoil peak larger than the one for the gas phase.

In figure 8, we present our liquid 5DCS (thick full line) for the separated contributions of the $1B_1$ and $2A_1$ orbitals compared to recent calculations for both liquid (thin full line) and gas (full diamonds) phases obtained within the FBA-CW (first born approximation-Coulomb wave) model [19]. This approximation is rather similar to ours but differs in the description of the molecular bound states. In the FBA-CW calculations, the water orbitals are described in a simpler manner by using a monocentric development of Gaussian expansions. For the computations in the liquid phase, the polarizable continuum approach is employed [50]. Our calculations exhibit a general good agreement with the liquid FBA-CW profiles in the whole angular domain. Even if this accord is better at the binary region, marked differences can be observed at backward emission angles. For instance, the FBA-CW model predicts lower cross sections than ours at the recoil region, giving differences of 30% for the $2A_1$ orbital. In this particular case, the deviations at the recoil region are more important if the static potential is included in our calculations (dashed–dotted lines). Experiments for gaseous water [14] are also included in figure 8. It is worth noting that the comparison is made only at the binary region where the measurement resolution is enough to separate the contribution of each orbital [14]. It is observed that the gas experimental data and the liquid results have the same shape at the binary region despite some differences in the magnitude of the structures. Gas 1CW cross sections (dotted line) are also included in the figures, showing appreciable deviations from ours for the liquid phase. Gas 1CW results are almost 50% (20%) lower at the binary region than the present ones for the liquid for the $1B_1$ [37] ($2A_1$) orbitals. This situation is quite different at the recoil region. For the $1B_1$ orbital, gas 1CW predictions are greater than ours for the liquid without static potential. However, the present calculations including it in the perturbation give an enhanced recoil peak comparable in magnitude to the one of the 1CW gas prediction. Considering the $2A_1$ orbital, our 5DCS present a more pronounced recoil peak than the ones predicted for the other models. Indeed, our model exhibits a recoil peak higher in magnitude than the binary one if the static potential is included in the calculations. It is worth mentioning that the FBA-CW model gives

cross sections that are barely distinguishable between both liquid and gas phases.

In figure 9, 5DCS for both the $1B_2$ and $1A_1$ inner orbitals are shown and compared with FBA-CW results for the liquid as well as with the experiments for the gas phase [14]. For the case of the $1B_2$ orbital, a behaviour similar to the $2A_1$ orbital is found: an overall good agreement is observed between our cross sections and the experiments for the gas, and also with the FBA-CW calculations for the liquid phase. Nevertheless, our model for the liquid gives cross sections with a recoil peak larger than the predicted ones by the other models. Concerning the inner $1A_1$ orbital, none of the theories presented here are able to predict the magnitude of either the binary or recoil peaks measured for the gas phase. Our liquid calculations seem to be in better accord with the 1CW calculations for the vapour [17].

4. Conclusions

We study the single ionization of water molecules from severals orbitals in the liquid phase by the impact of fast electrons through our first order model within an independent electron approximation [38]. This model introduces a novel feature for a proper characterization of the liquid phase: the bound states of a single water molecule in the liquid are obtained as expansions of the maximum localized Wannier functions [40, 41].

From the present results, we can extract several conclusions. First, the computed MDCS for the four external water orbitals are found to depend markedly on both the molecular orientation and the initial electronic configurations. Second, integrated cross sections over all molecular orientations show the expected physical features (such as binary and recoil peaks) observed in experiments for vapour [14]. The inclusion of a static short-range potential coming from the presence of the passive electrons does not change these characteristics. These findings validate the use of the present orbitals obtained through Wannier techniques for the computation of MDCS.

Finally, a good agreement between our calculations and the FBA-CW predictions for liquid water [19] is found, especially at the binary region. However, our model predicts higher cross sections at backward angles and the discrepancies are more important for the $2A_1$ orbital. This situation becomes more evident if the static potential is included in the calculations. Similar considerations can be obtained from the comparison between our liquid results and those for the gas phase [17, 19]. This fact suggests that the repulsion between the active electron and the passive ones may play an important role in the description of the averaged cross sections in particular in the recoil region. Moreover, the internal $2A_1$ and $1B_2$ orbitals seem to be more sensitive to the static potential. Unfortunately, no experiments are available at present to contrast with our predictions for the aqueous phase. Clearly, measurements of secondary electron emission from liquid targets still remains an elusive task for experimentalists. However, the new techniques allowing the determination of fragmentation yields for secondary ion emission from liquid water and ethanol [1–5] reveals a promising tool to measure ejected electrons from aqueous targets in the near future. Concerning this point, our work may serve to promote these kind of experiments. According to the trend of our results for angular distributions, it seems that liquid water and vapour despite a similar qualitative behaviour could present significant differences at least for the most external orbitals. However, at the current stage of our research we cannot establish if this may affect in an important way the integrated or total cross sections. Therefore, it would be interesting to pursue our investigations to obtain total cross sections, or even cross sections integrated over energy or angles of the ejected electron and check if these differences are still visible. Work in this direction is in progress.

Acknowledgments

Authors acknowledge financial support from the Agencia Nacional de Promoción Científica y Tecnológica (PICT No. 2145), and the Consejo Nacional de Investigaciones Científicas y Técnicas de la República Argentina (PIP No. 11220090101026).

References

[1] Kaneda M, Sato S, Shimizu M, He Z, Ishii K, Tsuchida H and Itoh A 2007 *Nucl. Instrum. Methods* B **256** 97
[2] Kaneda M, Shimizu M, Hayakawa T, Nishimura A, Iriki Y, Tsuchida H, Imai M, Shibata H and Itoh A 2009 *Nucl. Instrum. Methods* B **267** 908
[3] Shimizu M, Hayakawa T, Kaneda M, Tsuchida H and Itoh A 2009 *J. Phys.: Conf. Ser.* **194** 132038
[4] Kaneda M, Shimizu M, Hayakawa T, Iriki Y, Tsuchida H and Itoh A 2010 *J. Chem. Phys.* **132** 144502
[5] Itoh A, Kaneda M, Shimizu M, Hayakawa T, Iriki T and Tsuchida H 2010 *Vacuum* **84** 999
[6] Faubel M, Schlemmer S and Toennies J P 1988 *Z. Phys.* D **10** 269
[7] Winter B and Faubel M 2006 *Chem. Rev.* **106** 1193
[8] Opal C B, Beaty E C and Peterson W K 1972 *Data* **4** 209
[9] Vroom D A and Palmer R L 1977 *J. Chem. Phys.* **66** 3720
[10] Bolorisadeh M A and Rudd M E 1986 *Phys. Rev.* A **33** 882
[11] Hollman K W, Kerby G W III, Rudd M E, Miller J H and Manson S T 1988 *Phys. Rev.* A **38** 3299
[12] Straub H C, Lindsay B G, Smith K A and Stebbings R F 1998 *J. Chem. Phys.* **108** 109
[13] Champion C *et al* 2001 *Phys. Rev.* A **63** 052720
Champion C *et al* 2005 *Phys. Rev.* A **72** 059906
[14] Milne-Brownlie D S *et al* 2004 *Phys. Rev.* A **69** 032701
[15] Itikawa Y and Mason N G 2005 *J. Phys. Chem. Ref. Data* **34** 1
[16] Frémont F, Hajaji A, Chesnel J-Y, Leprince P, Porée F, Gervais B and Hennecart D 2006 *Phys. Rev.* A **74** 012717
[17] Champion C, Dal Cappello C, Houamer S and Mansouri A 2006 *Phys Rev.* A **73** 012717
[18] Kaiser C, Spieker D, Gao J, Hussey M, Murray A and Madison D H 2007 *J. Phys. B: At. Mol. Opt. Phys.* **40** 2563
[19] Champion C 2010 *Phys. Med. Biol.* **55** 11
[20] Sahlaoui M and Bouamoud M 2012 *J. Phys. B: At. Mol. Opt. Phys.* **45** 085201

[21] Nandi S, Biswas S, Khan A, Monti J M, Tachino C A, Rivarola R D, Misra D and Tribedi L C 2012 *Phys. Rev.* A **87** 052710
[22] Sahlaoui M, Bouamoud M, Lasri B and Dogan M 2013 *J. Phys. B: At. Mol. Opt. Phys.* **46** 115206
[23] Champion C *et al* 2013 *Nucl. Instrum. Methods* B **306** 165
[24] de Vera P, Garcia-Molina R, Abril I and Solov'yov A V 2013 *Phys. Rev. Lett.* **110** 148104
[25] Tachino C A, Monti J M, Fojón O A, Champion C and Rivarola R D 2014 *J. Phys. B: At. Mol. Opt. Phys.* **47** 035203
[26] Fernández-Menchero L and Otranto S 2014 *J. Phys. B: At. Mol. Opt. Phys.* **47** 035205
[27] Monti J M, Tachino C A, Hanssen J, Fojón O A, Galassi M E, Champion C and Rivarola R D 2014 *Appl. Radiat. Isot.* **83B** 105
[28] Quinto M A, Monti J M, Galassi M E, Weck P F, Fojón O A, Hanssen J, Rivarola R D and Champion C 2015 *J. Phys.: Conf. Ser.* **583** 012049
[29] de Vera P, Garcia-Molina R and Abril I 2015 *Phys. Rev. Lett.* B **114** 018101
[30] Nikjoo H, Goodhead D T, Charlton D E and Paretzke H G 1991 *Int. J. Radiat. Biol.* **60** 739
[31] Joshipura K N, Gangopadhyay S, Limbachiya C G and Vinodkumar M 2007 *J. Phys.: Conf. Ser.* **80** 012008
[32] Hafied H, Eschenbrenner A, Champion C, Ruiz-López R F, Dal Cappello C, Charpentier I and Hervieux P-A 2007 *Chem. Phys. Lett.* **439** 55
[33] Emetzoglou D, Nikjoo H, Pathak A and Sathish N 2007 *Nucl. Instrum. Methods* B **257** 609
[34] Bernal M and Liendo J 2007 *Nucl. Instrum. Methods* B **262** 1
[35] Bousis C, Emetzoglou D, Hadjidoukas P, Nikjoo H and Pathak A 2008 *Nucl. Instrum. Methods* B **266** 1185
[36] Siiskonen T, Kettunen H, Peräjärvi K, Javanainen A, Rossi M, Trzaska W H, Turunen J and Virtanen A 2011 *Phys. Med. Biol.* **56** 2367
[37] Fojón O A, de Sanctis M L, Vuilleumier R, Stia C R and Politis M-F 2011 *J. Phys.: Conf. Ser.* **288** 012010
[38] de Sanctis M L, Politis M-F, Vuilleumier R, Stia C R and Fojón O A 2012 *J. Phys. B: At. Mol. Opt. Phys.* **45** 045206
[39] Garcia-Molina R, Abril I, de Vera P and Paul H 2013 *Nucl. Instrum. Methods* B **299** 51
[40] Vuilleumier R and Sprik M 2001 *J. Chem. Phys.* **115** 3454
[41] Hunt P, Sprik M and Vuilleumier R 2003 *Chem. Phys. Lett.* **376** 68
[42] Marzari N and Vanderbilt D 1997 *Phys. Rev.* B **56** 12847
[43] Silvestrelli S, Marzari N, Vanderbilt D and Parrinello M 1998 *Solid State Commun.* **107** 7
[44] Champion C, Lekadir H, Galassi M E, Fojón O, Rivarola R D and Hanssen J 2010 *Phys. Med. Biol.* **55** 6053
[45] Stolterforht N, DuBois R D and Rivarola R D 1997 *Electron Emission in Heavy Ion-Atom Collisions* ed G Ecker, P Lambropoulos, I I Sobelman and H Walther (Berlin: Springer)
[46] Messiah A 1983 *Mecánica Cuántica* vol 2 (Madrid: Tecnos)
[47] Otranto S and Olson R E 2009 *Phys Rev.* A **80** 012714
[48] de Sanctis M L, Politis M-F, Vuilleumier R, Stia C R and Fojón O A 2015 *J. Phys.: Conf. Ser.* **583** 012023
[49] Slater J C 1930 *Phys. Rev.* **36** 57
[50] Tomasi J *et al* 2005 *Chem. Rev.* **105** 2999
[51] Moccia R 1964 *J. Chem. Phys.* **40** 2186